

Quenching of *para*-H₂ with an ultra-cold anti-hydrogen atom $\bar{\text{H}}_{1s}$

Renat A. Sultanov^{1*}, Sadhan K. Adhikari^{2†}, and Dennis Guster^{1‡}

¹*High Performance Computing Laboratory,*

St. Cloud State University,

St. Cloud, MN 56301-4498, USA

²*Institute of Theoretical Physics,*

UNESP – São Paulo State University,

01140-070 São Paulo, SP, Brazil

(Dated: February 13, 2022)

Abstract

In this work we report the results concerning calculations for quantum-mechanical rotational transitions in molecular hydrogen, H₂, induced by an ultra-cold ground state anti-hydrogen atom $\bar{\text{H}}_{1s}$. The calculations are accomplished using a non-reactive close-coupling quantum-mechanical approach. The H₂ molecule is treated as a rigid rotor. The total elastic scattering cross section $\sigma_{el}(\epsilon)$ at energy ϵ , state-resolved rotational transition cross sections $\sigma_{jj'}(\epsilon)$ between states j and j' and corresponding thermal rate coefficients $k_{jj'}(T)$ are computed in the temperature range $0.004 \text{ K} \lesssim T \lesssim 4 \text{ K}$. Satisfactory agreement with other calculations (variational) has been obtained for $\sigma_{el}(\epsilon)$.

PACS numbers:

* rasultanov@stcloudstate.edu; r.sultanov2@yahoo.com

† adhikari@ift.unesp.br, URL: <http://www.ift.unesp.br/users/adhikari/>

‡ dguster@stcloudstate.edu

I. INTRODUCTION

Interaction and collisional properties between matter and antimatter is of fundamental importance in physics [1, 2]. The anti-hydrogen atom $\bar{\text{H}}$, which is a bound state of an anti-proton p^- and a positron e^+ , is the simplest representative of an antimatter atom. This is a two-particle system, which, however, may possess very different interactional and dynamical properties compared to its matter counterpart the H atom [3, 4].

By now much effort has been exerted in various experiments to build and store $\bar{\text{H}}$ at cold and ultra-cold temperatures [5, 6, 7, 8, 9]. New experiments are planned or in progress to test the fundamental laws and theories of physics involving antiparticles and antimatter in general [2]. For example, it follows from the CPT symmetry of quantum electrodynamics that a charged particle and its anti-particle counterpart should have equal and opposite charges and equal masses, lifetimes and gyromagnetic ratios. The CPT symmetry predicts that hydrogen and anti-hydrogen atoms should have identical spectra. In this way experimentalists plan to test whether in fact H and $\bar{\text{H}}$ have such properties. Specifically, a starting point would be to compare the frequency of the 1s-2s two-photon transition in H and $\bar{\text{H}}$. Also, one of the important practical applications of antihydrogen has been mentioned in [10], where the authors considered controlled $\bar{\text{H}}$ propulsion for NASA's future plans in very deep space. Researchers at CERN [1] and from other groups [8] are interested to trap and study $\bar{\text{H}}$ at low temperatures, e.g., $T \lesssim 1$ K, when the $\bar{\text{H}}$ atom will be almost in its rest frame. The study of Lamb shift and response of antihydrogen to gravity at ultra-low energies should allow them to test more precisely the predictions of two fundamental theories of modern physics: quantum field theory and Einstein's general theory of relativity [11].

It has been pointed out that the main cause of loss of $\bar{\text{H}}$ atoms confined in a magnetic gradient trap is due to $\bar{\text{H}}+\text{H}_2$ and $\bar{\text{H}}+\text{He}$ collisions. Therefore, the $\bar{\text{H}}+\text{H}_2$ scattering cross-sections and corresponding rotational-vibrational thermal rate coefficients, in the case of H_2 , would be very helpful to gain a practical understanding of the slowing down and trapping of $\bar{\text{H}}$. Hence the investigation of the possibility of cooling of $\bar{\text{H}}$ atoms by colliding them with colder H_2 is of significant practical interest [12]. (Similar collision between trapped fermionic atoms with cold bosonic atoms has been fundamental in cooling the fermionic atoms and thus leading them to quantum degeneracy [13].) Such investigation of $\bar{\text{H}}$ interaction with H and H_2 can reveal the survival conditions of $\bar{\text{H}}$ in collisions with H and, even more importantly,

with H_2 [14].

Further, cooling occurs by energy transfer in elastic collisions of $\bar{\text{H}}$ with H_2 . However, during the collision the rearrangement process may lead to the formation of protonium (pp^-) and positronium (e^+e^-) exotic atoms and the destruction of $\bar{\text{H}}$ atoms. They are formed as matter-antimatter bound states, which then annihilate. (There have also been many studies of scattering of positronium atoms [15], the lightest matter-anti-matter atom). Thus one can conclude, that the effectiveness of cooling $\bar{\text{H}}$ is determined from a comparison of the cross sections for direct scattering and rearrangement.

By now a series of theoretical works have been published, in which the properties of interaction between $\bar{\text{H}}$ and H, He, H_2 have been investigated [16, 17, 18, 19]. Some theoretical studies have been carried out for the $\bar{\text{H}}+\text{H}$ system at thermal energies using quantum-mechanical methods [20, 21, 22, 23, 24, 25]. Also, discussions on the importance and applications for this system, especially, in connection with Bose-Einstein condensation [26], ultra-cold collisions [14, 21], and its static and dynamic properties [27], can be found in the literature.

In this work we present results for the collision of an ultra-cold $\bar{\text{H}}$ atom with H_2 , where H_2 is treated as a rigid rotor with a fixed distance between hydrogen atoms. The elastic, rotational state-resolved scattering cross sections for the $\bar{\text{H}}-\text{H}_2$ scattering and their corresponding thermal rate coefficients are calculated using a non-reactive quantum-mechanical close-coupling approach. The potential interaction between $\bar{\text{H}}$ and the hydrogen atoms is taken from Ref. [16].

In the next section we present the quantum-mechanical formalism used in this work. The results and discussion are presented in Sec. III. Conclusions are given in Sec. IV.

II. $\bar{\text{H}}-\text{H}_2$ SCATTERING FORMULATION

A. Basic Equations

In this section we describe the close-coupling quantum-mechanical approach we used to calculate the cross sections and collision rates of a hydrogen molecule H_2 with an anti-hydrogen atom $\bar{\text{H}}$. Atomic units ($e = m_e = \hbar = 1$) are used in this section, where e and m_e are charge and mass of an electron. Three-body Jacobi coordinates $\{\vec{r}, \vec{R}\}$ for the $\bar{\text{H}}+\text{H}_2(j)$

system used in this work are shown in Fig. 1. The two H atoms are labeled 2 and 3 and the $\bar{\text{H}}$ atom is labeled 1, O is the center of mass of the H_2 molecule, Θ is the polar angle between vector \vec{r} connecting the two H atoms in H_2 (labeled 2 and 3) and vector \vec{R} connecting the center of mass of the H_2 molecule to the $\bar{\text{H}}$ atom (labeled 1). Next, \vec{j} and \vec{L} are angular momenta corresponding to the vectors \vec{r} and \vec{R} , respectively. The quantities x_{21} and x_{31} are the distances between the $\bar{\text{H}}$ atom labeled 1 and the H atoms labeled 2 and 3, respectively.

The Schrödinger equation for an $a + bc$ collision in the center of mass frame, where a ($\bar{\text{H}}$) is an atom and bc ($\bar{\text{H}}_2$) is a linear rigid rotor, is [28, 29]

$$\left(\frac{P_{\vec{R}}^2}{2M_R} + \frac{L_{\hat{r}}^2}{2\mu r^2} + V(\vec{r}, \vec{R}) - E \right) \Psi(\hat{r}, \vec{R}) = 0. \quad (1)$$

where $P_{\vec{R}}$ is the relative momentum between a and bc , M_R is the reduced mass of the atom-molecule (rigid rotor in this model) system $a + bc$: $M_R = m_a(m_b + m_c)/(m_a + m_b + m_c)$, μ is the reduced mass of the target: $\mu = m_a m_b/(m_a + m_b)$, \hat{r} is the angle of orientation of the rotor ab , $V(\vec{r}, \vec{R})$ is the potential energy surface (PES) for the three-atom system abc , and E is the total energy of the system. The eigenfunctions of the operator $L_{\hat{r}}^2$ in Eq. (1) are the spherical harmonics $Y_{jm}(\hat{r})$.

To solve Eq. (1), the following expansion is used [30]

$$\Psi(\hat{r}, \vec{R}) = \sum_{JMjL} \frac{U_{jL}^{JM}(R)}{R} \phi_{jL}^{JM}(\hat{r}, \vec{R}), \quad (2)$$

where channel expansion functions are

$$\phi_{jL}^{JM}(\hat{r}, \vec{R}) = \sum_{m_1 m_2} C_{j m_1 L m_2}^{JM} Y_{j m_1}(\hat{r}) Y_{L m_2}(\hat{R}), \quad (3)$$

here $\vec{J} = \vec{j} + \vec{L}$ is the total angular momentum of the system abc , and M is its projection onto the space fixed z axis, m_1 and m_2 are projections of j and L respectively, $C_{j m_1 L m_2}^{JM}$ are the Clebsch-Gordan coefficients, and U 's are the appropriate radial functions.

Substitution of Eq. (2) into Eq. (1) provides a set of coupled second order differential equations for the unknown radial functions $U_{jL}^{JM}(R)$

$$\left(\frac{d^2}{dR^2} - \frac{L(L+1)}{R^2} + k_{jL}^2 \right) U_{jL}^{JM}(R) = 2M_R \sum_{j'L'} \int \langle \phi_{jL}^{JM}(\hat{r}, \vec{R}) | V(\vec{r}, \vec{R}) | \phi_{j'L'}^{JM}(\hat{r}, \vec{R}) \rangle \times U_{j'L'}^{JM}(R) d\hat{r} d\hat{R}. \quad (4)$$

To solve the coupled radial equations (4), we apply the hybrid modified log-derivative-Airy propagator in the general purpose scattering program MOLSCAT [31]. Additionally, we

tested other propagator schemes included in MOLSCAT. Our calculations reveal that other propagators can also produce quite stable results.

The log-derivative matrix is propagated to large intermolecular distances R , since all experimentally observable quantum information about the collision is contained in the asymptotic behavior of functions $U_{jL}^{JM}(R \rightarrow \infty)$. The numerical results are matched to the known asymptotic behavior of $U_{jL}^{JM}(R)$ relating to the physical scattering S -matrix [32]

$$U_{jL}^{JM} \underset{R \rightarrow +\infty}{\sim} \delta_{jj'} \delta_{LL'} e^{-i(k_\alpha R - (L\pi/2))} - \left(\frac{k_\alpha}{k_{\alpha'}} \right)^{1/2} S^J(j'L'; jL; E) e^{i(k_{\alpha'} R - (L'\pi/2))}, \quad (5)$$

where $k_\alpha = [2M_R(E - E_\alpha)]^{1/2}$ is the channel wave-number of channel $\alpha = (jL)$, E_α is rotational channel energy and E is the total energy in the abc system. This method was used for each partial wave until a converged cross section was obtained. It was verified that the results have converged with respect to the number of partial waves as well as the matching radius, R_{max} , for all channels included in our calculations.

Cross sections for rotational excitation and relaxation phenomena can be obtained directly from the S -matrix. In particular, the cross sections for excitation from $j \rightarrow j'$ summed over the final m' and averaged over the initial m are given by [30]

$$\sigma(j', j, \epsilon) = \frac{\pi}{(2j+1)k_\alpha^2} \sum_{JLL'} (2J+1) |\delta_{jj'} \delta_{LL'} - S^J(j'L'; jL; E)|^2. \quad (6)$$

The kinetic energy is $\epsilon = E - B_e j(j+1)$, where B_e is the rotation constant of the rigid rotor bc , i.e. the hydrogen molecule.

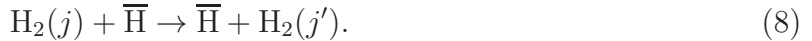
The relationship between the rate coefficient $k_{j \rightarrow j'}(T)$ and the corresponding cross section $\sigma_{j \rightarrow j'}(E_{kin})$ can be obtained through the following weighted average [33]

$$k_{j \rightarrow j'}(T) = \frac{8k_B T}{\pi M_R} \frac{1}{(k_B T)^2} \int_{\epsilon_s}^{\infty} \sigma_{j \rightarrow j'}(\epsilon) e^{-\epsilon/k_B T} \epsilon d\epsilon, \quad (7)$$

where $\epsilon = E - E_j$ is pre-collisional translational energy at temperature T , k_B is Boltzman constant, and ϵ_s is the minimum value of the kinetic energy needed to make E_j levels accessible.

B. $\overline{\text{H}}\text{-H}_2$ Interaction Potential

In the following section, we will present our results for rotational quantum transitions in collision between H_2 and an anti-hydrogen atom $\overline{\text{H}}$, that is



Here H_2 is treated as a vibrationally averaged rigid monomer rotor. The bond length was fixed at 1.449 a.u. or 0.7668 Å. The rotation constant of the H_2 molecule has been taken as $B_e = 60.8\text{cm}^{-1}$. The H_2 rigid rotor model has been already applied in different publications [30, 34, 35, 36, 37, 38, 39, 40]. For the considered range of kinetic energies the model can be quite justified in this special case when only pure rotational quantum transitions at low collisional energies are of interest as in $\text{H}_2(j)+\overline{\text{H}}$, and when the energy gap between rotational and vibrational energies is much larger than kinetic energy of collision. In such a model the quantum mechanical approach is rather simplified.

Next we consider an important physical parameter in atomic and molecular collisions, e. g., the PES between the atoms. There is no global potential energy surface available for the three-atom $\overline{\text{H}}\text{-H}_2$ system. However in Ref. [16], the author calculated the values of interaction energy between H and $\overline{\text{H}}$, i. e., the $\text{H}\text{-}\overline{\text{H}}$ energy curve using the Rayleigh-Ritz variational method. Further, the microHartree accuracy of Born-Oppenheimer energies of the system has been achieved in that work.

To construct the $\text{H}_2\text{-}\overline{\text{H}}$ interaction potential we take the $\text{H}\text{-}\overline{\text{H}}$ energy data from Ref. [16] and make a cubic spline interpolation through all 46 points taken from Table 1 of that paper. These data have been tabulated from $R_{min} = 0.744$ a.u. to $R_{max} = 20.0$ a.u. inter-atomic distances. Because in the current work we use the rigid rotor model for H_2 , we do not need the interaction energy between hydrogen atoms in H_2 . The interaction potential between a hydrogen molecule and $\overline{\text{H}}$ is taken by sandwiching the two $\overline{\text{H}}\text{-H}$ potential energy curves:

$$V(\vec{r}, \vec{R}) = V(r, R, \Theta) = V_{\text{H}\text{-}\overline{\text{H}}}^{21}(x_{21}) + V_{\text{H}\text{-}\overline{\text{H}}}^{31}(x_{31}), \quad (9)$$

where distances between atoms are written as follow (cf. Fig. 1):

$$x_{21} = \sqrt{r^2/4 + R^2 + rR \cos \Theta} \quad \text{and} \quad x_{31} = \sqrt{r^2/4 + R^2 + rR \cos(\pi - \Theta)}. \quad (10)$$

The functions $V_{\text{H}\text{-}\overline{\text{H}}}^{k1}(y)$ with $k = 2(3)$ are represented as cubic spline interpolation func-

tions for any value of $y = x_{21}$ or $y = x_{31}$ as follows:

$$V_{\overline{\text{H}}-\text{H}}^{k1}(y) = V_{\overline{\text{H}}-\text{H}}^{k1}(X_i) + B_i(y - X_i) + C_i(y - X_i) + D_i(y - X_i), \quad (11)$$

where $B_i(y - X_i)$, $C_i(y - X_i)$, $D_i(y - X_i)$ perform the spline interpolation and where $X_i \leq y \leq X_{i+1}$, in each sub-interval $[X_i, X_{i+1}]$, $i = 1, 2, 3, \dots, (n - 1)$, $n = 46$. The coordinates X_i and corresponding values of the $\text{H}-\overline{\text{H}}$ potential energy data have been taken from Table 1 of Ref. [16].

The calculated PES is shown in Fig. 2. It is clear that the potential has a singular value when the distance between $\overline{\text{H}}$ and H_2 is equal to zero. Additionally, the $\overline{\text{H}}-\text{H}_2$ PES which we obtain from Eq. (9) is shown in Fig. 3. Specifically, this potential was used in our calculations of $\overline{\text{H}} + \text{H}_2$ collisions. Again, as seen in Fig. 2 the potential energy curve between $\overline{\text{H}}-\text{H}$ has a Coulomb type singularity at small distances. In our calculations we needed to make additional test runs to achieve convergence in our results. In the next section we will briefly demonstrate the numerical convergence of the results when calculating total elastic scattering cross sections. These results depend on various numerical and quantum-mechanical scattering parameters.

III. RESULT AND DISCUSSION

A. Convergence test

Numerous test calculations have been undertaken to insure the convergence of the results with respect to all parameters that enter in the propagation of the Schrödinger equation. These include the atomic-molecular distance R , the total angular momentum J , the number of total rotational levels to be included in the close-coupling expansion and others, see Fig. 1. Particular attention has been given to the total number of numerical steps in the propagation over the distance R of the Schrödinger equation (4). Specifically, the parameter R ranges from 0.75 a.u. to 20.0 a.u. We used up to 50000 propagation points. We also applied and tested different mathematical propagation schemes included in MOLSCAT.

The rotational energy levels of *para*- $\text{H}_2(j)$ and the corresponding angular momenta j are shown in Table I. The goal of this work is to get new results for $\overline{\text{H}} + \text{para}-\text{H}_2$ thermal rate coefficients $k_{j \rightarrow j'}(T)$ at ultra-low temperatures: specifically $0.004 \text{ K} < T < 4 \text{ K}$. The corresponding cross sections have been calculated for collision energies varying from ~ 0.0001

cm^{-1} to $\sim 100 \text{ cm}^{-1}$. These energy values are very small. However, despite this fact, to reach convergence of the results we needed to include in expansion (2) a significant number of rotational levels of the H_2 molecule, specifically up to $j_{max} \approx 60$. Below in Table II we present these results.

Also, we found that, at lower energies, for the numerical solution of Eq. (4) a much larger number of propagation (integration) points are needed than at higher energies. Specifically, at higher energies we need 500 propagation points, but for lower energies 50,000 points are needed to achieve comparable precision. Convergence has been achieved for elastic scattering cross sections for various scattering parameters. Below in Table III we present these results. Then we used this data in our calculation for rotational energy transfer, elastic scattering cross section and thermal rate coefficient.

Now in Table II we present results for the total elastic cross sections for two collisional energies: 0.1 cm^{-1} and 0.01 cm^{-1} . The cross sections are shown for a number of different maximum values of the rotational angular momentum $j = j_{max}$ in the H_2 molecule included in expansion (2). This is also the JMAX parameter in MOLSCAT [31]. Other scattering parameters have also been treated correctly in the calculation. One can see that JMAX should be at least 56. The other scattering parameter in Table II is MXSYM [31]. It reflects the number of terms in the potential expansion over angular functions [29, 30]. It is therefore evident that in this calculation we need to keep at least 24 terms in the expansion.

In Table III we also present results for total elastic scattering cross sections for few more selected energies. However in this table the convergence has been reached by increasing the total angular momentum J and by increasing the total number of the propagation steps in the propagation over the coordinate R of the Schrödinger equation (4). As expected, for lower energy collision we needed smaller values for the maximum J . For example, for collision energy $E_{coll} = 0.01 \text{ a.u.}$ it is enough to have $J = 0$, however $J = 10$ should be taken for $E_{coll} = 100.0 \text{ a.u.}$

In regard to the total number of the propagation steps in the solution of Eq. (4) one can see, that we need to include many more propagation points for low energy calculations. All test calculations in Table III have been done with JMAX = 56 and MXSYM = 24. The obtained results concerning the numerical and scattering parameters have been used in our calculation for total elastic $\sigma_{el}(E)$ and rotational quantum state transfer $\sigma_{j \rightarrow j'}(E)$ cross sections and corresponding thermal rate coefficients $k_{j \rightarrow j'}(T)$.

B. $\bar{\text{H}} + \text{para-H}_2$ results

Now we present computational results for process (8), namely, for elastic scattering ($j = 0 \rightarrow j' = 0$) and for low quantum number rotational transition between levels with $j = 0, 2$ and 4 : $2 \rightarrow 0$, $0 \rightarrow 2$, $4 \rightarrow 0$, and $4 \rightarrow 2$. From the results of Table III we see that to reach numerical convergence, for example, for the elastic scattering cross section, we need to include a large number of H_2 rotational levels, specifically up to 60.

The results for the elastic scattering cross sections $\sigma_{el}(\epsilon)$ for $\bar{\text{H}} + \text{H}_2 \rightarrow \text{H}_2 + \bar{\text{H}}$ are shown in Fig. 4 together with the corresponding results of variational calculations of Gregory and Armour [14]. It can be seen, that basically the two sets of cross sections are close to each other, although in our calculation we use larger number of collision energy points, specifically up to 200. In our calculation a shape resonance is found at energy $\epsilon \sim 3.5 \times 10^{-5}$ Hartree. As in Ref. [14] our $\sigma_{el}(\epsilon)$ tends to reach a constant value at lower energies with $\sigma_{el}(\epsilon \lesssim 10^{-8} \text{ a.u.}) = 9.47 \times 10^3 a_0^2$. This result allows us to calculate the $\bar{\text{H}} + \text{H}_2$ scattering length, which is

$$a = \sqrt{\sigma_{el}/(4\pi)} = 27.5 a_0. \quad (12)$$

The Gregory-Armour scattering length [14] obtained with a variational method is $\tilde{a} = 19.5 a_0$. The two results are in reasonable agreement with each other.

In Fig. 5 (a) and (b) we show the total state-resolved cross sections $\sigma_{j=2 \rightarrow j'=0}(v)$ vs. velocity v and the corresponding thermal rate coefficients $k_{2 \rightarrow 0}(T)$ vs. temperature T for the hydrogen molecule rotational relaxation process. It is seen, that when the collision energy increases the de-excitation cross section decreases. It can be explained in the following way: at low relative velocities (kinetic energies) between $\text{H}_2(j = 2)$ and $\bar{\text{H}}$, the rotationally excited H_2 molecule has more time for interaction and consequently, it has higher quantum-mechanical probability to release its internal rotational energy to $\bar{\text{H}}$. The resulting corresponding rate coefficients have been calculated for a temperature range from $0.004 \text{ K} < T < 4 \text{ K}$ and are also presented in Fig. 5 below the cross section results.

Next, in Fig. 6 (a) and (b) we present results for the total state-resolved cross sections $\sigma_{0 \rightarrow j'=2}(v)$ vs. velocity v and the corresponding thermal rate coefficients $k_{0 \rightarrow 2}(T)$ vs. temperature T for the hydrogen molecule rotational excitation process. It is quite understandable, as we find from Fig. 6 (a), that when the collision energy (relative velocity v) is increases the quantum-mechanical probability and corresponding cross section of the rotational excitation

of $H_2(j)$ are also increases. Figure 6 (b) depicts the corresponding results for the thermal rate coefficient.

In Figs. 7 (a) and (b) we present results for cross sections and rates for rotational relaxation process, as in Figs. 5 (a) and (b), but now connecting the states $j = 4$ and $j' = 2$. Finally, in Figs. 8 (a) and (b) we present results for cross sections and rates for rotational relaxation process but now connecting the states $j = 4$ and $j' = 0$. An unexpected result has been found in Fig. 7 (a) in the rotational transition cross section $\sigma_{4 \rightarrow 2}(v)$, i.e., when the H_2 quantum angular momentum has been changed from $j = 4$ to $j' = 2$. One can see, that the values of these cross sections at very low collision energies are almost from 5 to 10 times larger than other cross sections considered in this work, compare with the results from Figs. 5, 6 and 8.

IV. SUMMARY

A quantum-mechanical study of the state-resolved rotational relaxation and excitation cross sections and thermal rate coefficients in ultra-cold collisions between hydrogen molecules H_2 and anti-hydrogen atoms \bar{H} has been the subject of this work. A model PES for $H_2\text{-}\bar{H}$ has been constructed by sandwiching two $H\text{-}\bar{H}$ interaction potentials for two different hydrogen atoms taken from Ref. [16]. This $H\text{-}\bar{H}$ interaction potential is shown in Fig. 2. The $H_2\text{-}\bar{H}$ PES is presented in Fig. 3. Calculation for total elastic scattering cross section and for low quantum rotational transition states have been performed. We considered only the following quantum transitions: $2 \rightarrow 0$, $0 \rightarrow 2$, $4 \rightarrow 2$, and $4 \rightarrow 0$.

A test of the numerical convergence was undertaken. These results are presented in Tables II and III. Our results reveal that it is necessary to set the rotational angular momentum j_{max} in the H_2 molecule to a relatively large number, i.e. in the expansion (2) we needed to include up to 60 terms. The calculation was performed using the MOLSCAT program [31]. Different propagation schemes included in the MOLSCAT program have been used and tested. Additionally, the MXSYM potential parameter in that program also needed to have a relatively large value to obtain good convergence as can be seen from Table II. The numerical convergence has also been tested over the total number of the propagation steps over coordinate R in the solution of the Schrödinger equation (4). We have found, that at low energies we need a much larger number of integration points than at higher

energies, cf. Table III. Our results for the $\text{H}_2(j)+\bar{\text{H}}$ total elastic scattering cross section are in reasonable agreement with the corresponding results from Gregory and Armour [14]. The authors of this paper used a different PES, which is still unpublished, and applied a quantum-mechanical variational approach. Unfortunately, the rotational transitions in the $\text{H}_2(j)+\bar{\text{H}}$ collisions have not been calculated in that work [14]. One of the interesting results of the present work is that the cross section of the rotational transitions from $\text{H}_2(j = 4 \rightarrow j = 2)$ at ultra-low energies are approximately 5-10 times larger than other transition state cross sections.

To the best of our knowledge we do not know of any other calculation of the rotational transitions in the $\text{H}_2(j)+\bar{\text{H}}$ collision. These results can help to model energy transfer processes in the hydrogen-anti-hydrogen plasma, and perhaps to design new experiments in the field of the anti-hydrogen physics. Finally, we believe, that in the future work it should be useful to include vibrational degrees of freedom of the H_2 molecules, i.e. to carry out quantum-mechanical calculations for different rotational-vibrational relaxation processes: $\text{H}_2(v, j) + \bar{\text{H}} \rightarrow \bar{\text{H}} + \text{H}_2(v', j')$, where v and v' are the vibrational quantum numbers of H_2 before and after the collision, respectively.

ACKNOWLEDGMENT

This work was supported by St. Cloud State University internal grant program and CNPq and FAPESP of Brazil.

-
- [1] R. Landua, Phys. Rep. 403, 323 (2004).
 - [2] M. H. Holzscheiter, M. Charlton, and M.M. Nieto, Phys. Rep. 402, 1 (2004).
 - [3] A. Yu. Voronin, P. Froelich, B. Zygelma, Physical Review A 72, 062903 (2005).
 - [4] A. Yu. Voronin, P. Froelich, J. Phys. B 38, L301 (2005).
 - [5] G.P. Collins, Sci. Amer. 292, 78 (2005).
 - [6] M. Amoretti et al., Nature 419 (6906) 456 (2002).
 - [7] T.W. Hijmans, Nature 419, 439 (2002).
 - [8] G. Gabrielse, Advan. Atom., Molec. and Opt. Phys. 50, 155 (2005).
 - [9] G. Gabrielse *et al.* Phys. Rev. Lett. 89, 213401 (2002); 89, 233401 (2002).
 - [10] M.M. Nieto, M.H. Holzscheiter and S.G. Turyshev, arXiv:astro-ph/0410511v1, 21 Oct 2004.

- [11] M.H. Holzscheiter and M. Charlton, Rep. Prog. Phys. 62, 1 (1999).
- [12] J.S. Cohen, J. Phys. B 39 (17) 3561 (2006).
- [13] S. Giorgini *et al.*, Rev. Mod. Phys. **80**, 1215 (2008).
- [14] M.R. Gregory, E.A.G. Armour, Nucl. Instrum. Meth. in Phys. Res. B 266, 374 (2008).
- [15] P. K. Biswas and S. K. Adhikari, Chem. Phys. Lett. **317**, 129 (2000); J. Phys. B **33**, 1575 (2000); **31**, L315 (1998); S. K. Adhikari and P. K. Biswas, Phys. Rev. A **59**, 2058 (1999); S. K. Adhikari, P. K. Biswas and R. A. Sultanov, *ibid.* **59**, 4829 (1999).
- [16] K. Strasburger, J. Phys. B **35**, L435 (2002).
- [17] K. Strasburger and H. Chojnacki, Phys. Rev. Lett. 88, 163201 (2002).
- [18] K. Strasburger, J. Phys. B 37, 4483 (2004).
- [19] K. Strasburger, J. Phys. B: Atomic, Molecular and Optical Physics, 38 (17) 3197 (2005).
- [20] E.A.G. Armour and V. Zeman, Int. J. Quantum Chem. 74, 645 (1999).
- [21] P.K. Sinha and A.S. Ghosh, Europhys. Lett. 49, 558 (2000).
- [22] V. Zeman, E.A.G. Armour, and R.T. Pack, Phys. Rev. A 61, 052713 (2000)
- [23] S. Jonsell, A. Saenz, P.Froelich, B. Zygelman, A. Dalgarno, Phys. Rev. A 64, 052712 (2001).
- [24] E.A.G. Armour and C.W. Chamberlain, J. Phys. B 35, L489 (2002)
- [25] P.K. Sinha, P. Chaudhuri, and A.S. Ghosh, Phys. Rev. A 67, 052509 (2003).
- [26] M. M. Nieto, M. H. Holzscheiter, and T. J. Phillips, J. Optics B 5, S547 (2003).
- [27] L. Labzowsky, D. Solovyev, V. Sharipov, G. Plunien, and G. Soff, J. Phys. B 36, L227 (2003); C. Y. Hu and D. Caballero, *ibid.* 35, 3879 (2002); E. Cubero, M. Orozco, P. Hobza, and F. J. Luque, J. Phys. Chem. A 103, 6394 (1999); P. Hobza, V. Spirko, Z. Havlas, K. Buchhold, B. Reimann, H. D. Barth, and B. Brutschy, Chem. Phys. Lett. 299, 180 (1999); P. Hobza and Z. Havlas, *ibid.* 303, 447 (1999).
- [28] A.M. Arthurs and A. Dalgarno, Proc. Roy. Soc. A 256, 540 (1963).
- [29] S. Green, J. Chem. Phys. 70, 4686 (1979).
- [30] S. Green, J. Chem. Phys. 62, 2271 (1975).
- [31] J.M. Hutson, S. Green, Molscat ver. 14 (Distributed by Collaborative Computational Project 6, Daresbury Laboratory, UK, England, Phys. Sci. Res. Council) (1994).
- [32] L.D. Landau, L.M. Lifshitz, Quantum Mechanics: Non-Relativistic Theory, third edition, vol. 3, Elsevier, Amsterdam, 1981.
- [33] G.D. Billing, K.V. Mikkelsen, Molecular Dynamics and Chemical Kinetics, Wiley-Interscience,

New York, 1996.

- [34] S. Green, *J. Chem. Phys.* 67, 715 (1977).
- [35] J. Schaefer, *Astron. Astrophys. Suppl. Ser.* 85, 1101 (1990).
- [36] D.R. Flower, *Mon. Not. R. Astron. Soc.* 297, 334 (1998).
- [37] E. Roueff, D.R. Flower, *Mon. Not. R. Astron. Soc.* 305, 353 (1999).
- [38] R.A. Sultanov, D. Guster, *Chem. Phys.* 326, 641 (2006). (Note that in Eq. (1) of this work the momentum operators should be squared and the equation should look as follows:
$$\left(\frac{P_{\vec{R}}^2}{2M_{12}} + \frac{L_{\hat{r}_1}^2}{2\mu_1 r_1^2} + \frac{L_{\hat{r}_2}^2}{2\mu_2 r_2^2} + V(\vec{r}_1, \vec{r}_2, \vec{R}) - E \right) \Psi(\hat{r}_1, \hat{r}_2, \vec{R}) = 0$$
, as Eq. (2) in [40].
- [39] R.A. Sultanov, D. Guster, *Chem. Phys. Lett.* 428, 227 (2006); 436, 19 (2007).
- [40] R.A. Sultanov, A.V. Khugaev, D. Guster, *Chem. Phys. Lett.* 475, 175 (2009).

TABLE I: *para*-H₂ rotational spectrum.

Level	Rotational energy (cm ⁻¹)	Internal quantum momentum in <i>para</i> -H ₂ (j)
1	0.00	0
2	364.80	2
3	1216.00	4
4	2553.60	6
5	4377.60	8
6	6688.00	10
7	9484.80	12
8	12768.00	14
9	16537.60	16
10	20793.60	18
11	25536.00	20
12	30764.80	22
13	36480.00	24
14	42681.60	26
15	49369.60	28
16	56544.00	30
17	64204.80	32
18	72352.00	34
19	80985.60	36
20	90105.60	38
21	99712.00	40
22	109804.80	42
23	120384.00	44
24	131449.60	46
25	143001.60	48
26	155040.00	50
27	167564.80	52
28	180576.00	54
29	194073.60	56

TABLE II: Convergence of the total elastic scattering cross section σ_{el} (10^{-16}cm^2) at different energies E (cm^{-1}) in $\overline{\text{H}}+\text{H}_2 \rightarrow \text{H}_2+\overline{\text{H}}$ with respect to the maximum value of the rotational angular momentum $j = j_{max}$ in $\text{H}_2(j)$ included in the expansion (2) (parameter JMAX in MOLSCAT). Convergence with the number of terms in the potential expansion (parameter MXSYM in MOLSCAT) is also shown. Numbers in parentheses are powers of 10.

E (cm^{-1})	$\sigma_{el} \times 10^{16}$ (cm^2)								
	JMAX					MXSYM			
	30	40	50	56	60	12	20	24	26
0.1	61.0	5.25(2)	1.59(3)	1.59(3)	1.59(3)	1.97(3)	1.61(3)	1.59(3)	1.59(3)
0.01	55.4	1.06(3)	6.59(3)	6.62(3)	6.62(3)	1.12(4)	6.75(3)	6.56(3)	6.54(3)

TABLE III: Convergence for the total elastic scattering cross section σ_{el} (10^{-16}cm^2) at different collision energies E in (cm^{-1}) in $\overline{\text{H}}+\text{H}_2 \rightarrow \text{H}_2+\overline{\text{H}}$ with respect to the maximum value of the total angular momentum J of the 3-atomic system: parameter JTOT in MOLSCAT. Convergence on the number of numerical space steps in propagation over distance R of the Schrödinger equation (parameter STEPS in MOLSCAT) is also shown. Numbers in parentheses are powers of 10.

E (cm^{-1})	$\sigma_{el} \times 10^{16}$ (cm^2)						
	JTOT			STEPS			
	0	2	-	500	1000	10000	50000
0.1	1.59(3)	1.59(3)		3.64(2)	2.67	1.60(3)	1.59(3)
0.01	6.62(3)	6.62(3)		3.62(2)	1.75(-1)	6.63(3)	6.62(3)
	4	6	8	500	1000	5000	7000
10.0	5.85(1)	5.96(1)	5.96(1)	6.23(1)	6.00(1)	5.96(1)	5.96(1)
1.0	1.69(2)	1.69(2)	-	1.77(2)	1.70(2)	1.70(2)	1.70(2)
	8	10	12	500	750	-	-
100.0	1.65(2)	1.72(2)	1.72(2)	1.72(2)	1.72(2)	-	-

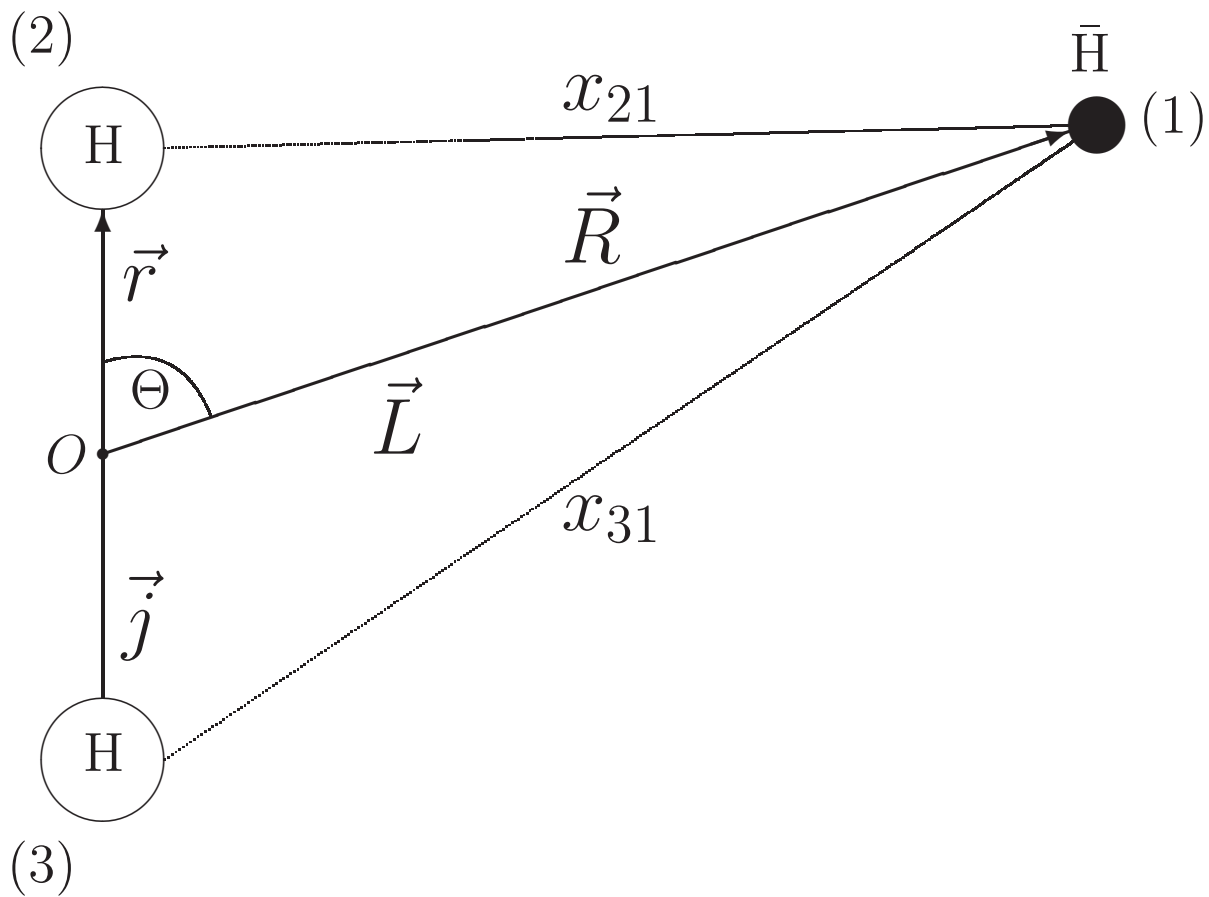


FIG. 1: Three-body Jacobi coordinates $\{\vec{r}, \vec{R}\}$ for the $\bar{\text{H}}+\text{H}_2(j)$ system used in this work.

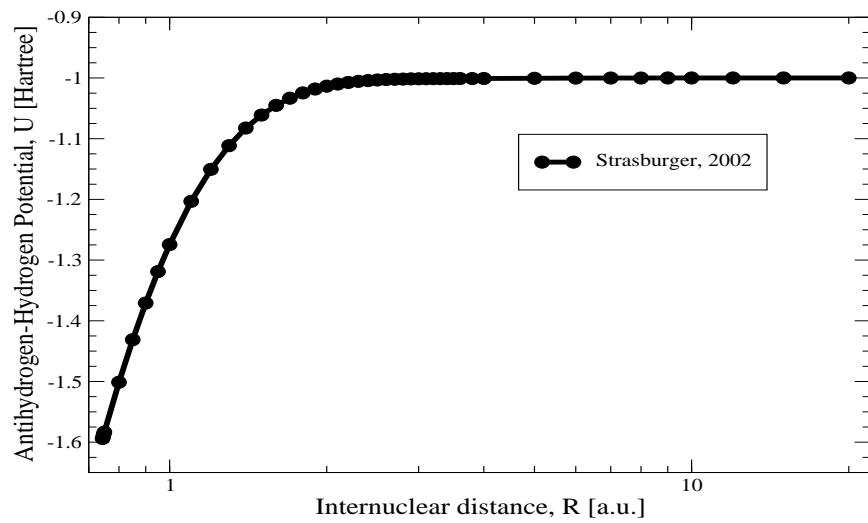


FIG. 2: $\bar{\text{H}}\text{-H}$ potential energy curve from Ref. [16]

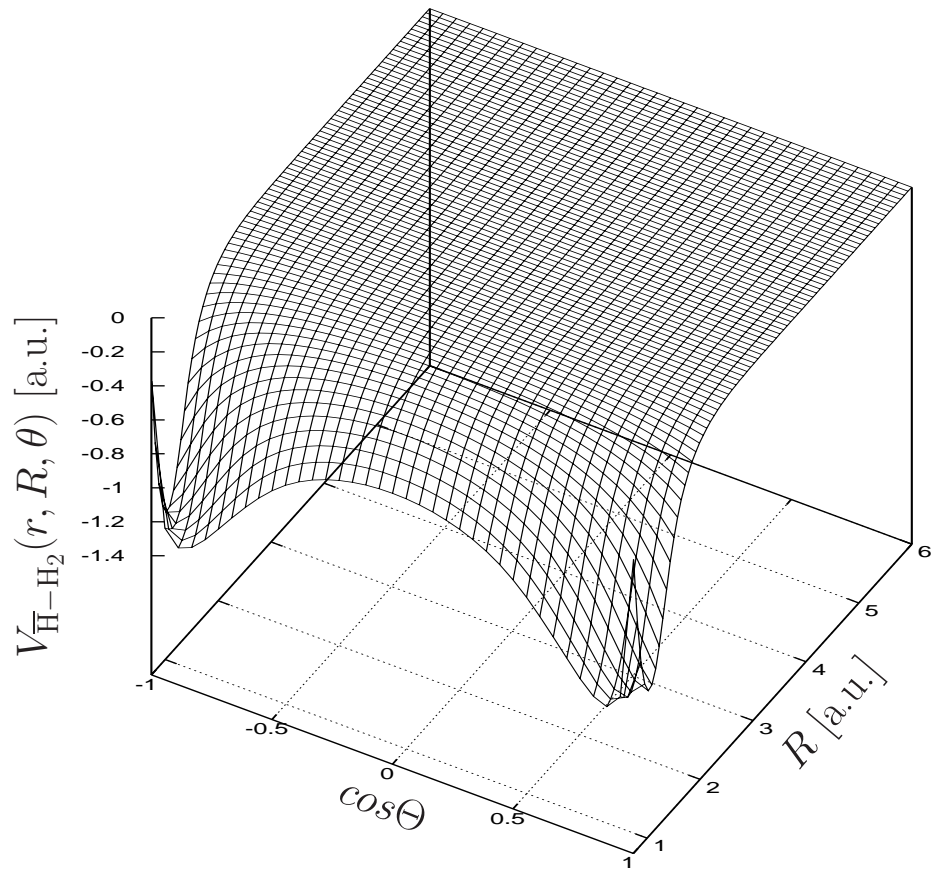


FIG. 3: Interaction potential $V_{\bar{H}-H_2}(r, R, \theta)$ between \bar{H} and H_2 in a.u. The distance between hydrogen atoms in H_2 is fixed at $r = r(H_2) = 1.409$ a.u.

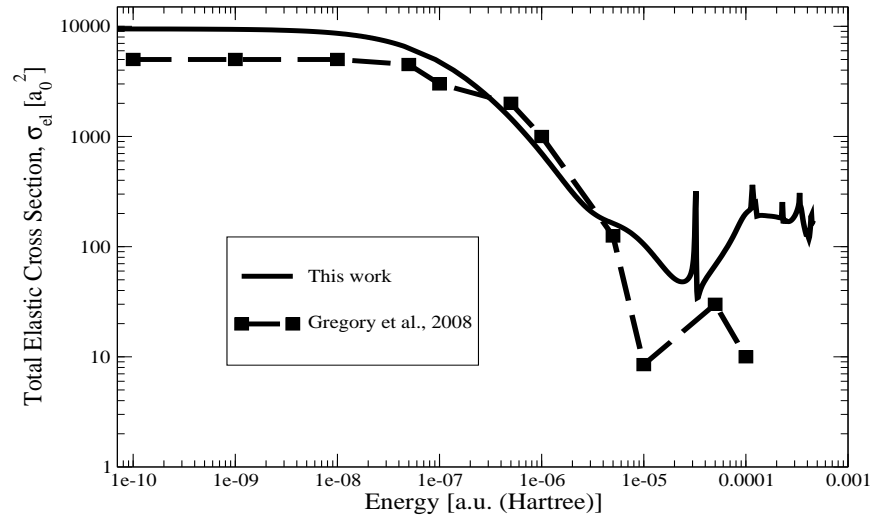


FIG. 4: Total elastic scattering cross section for $\bar{\text{H}} + \text{H}_2$ at different energies: results from Gregory *et al.* [14] and this work.

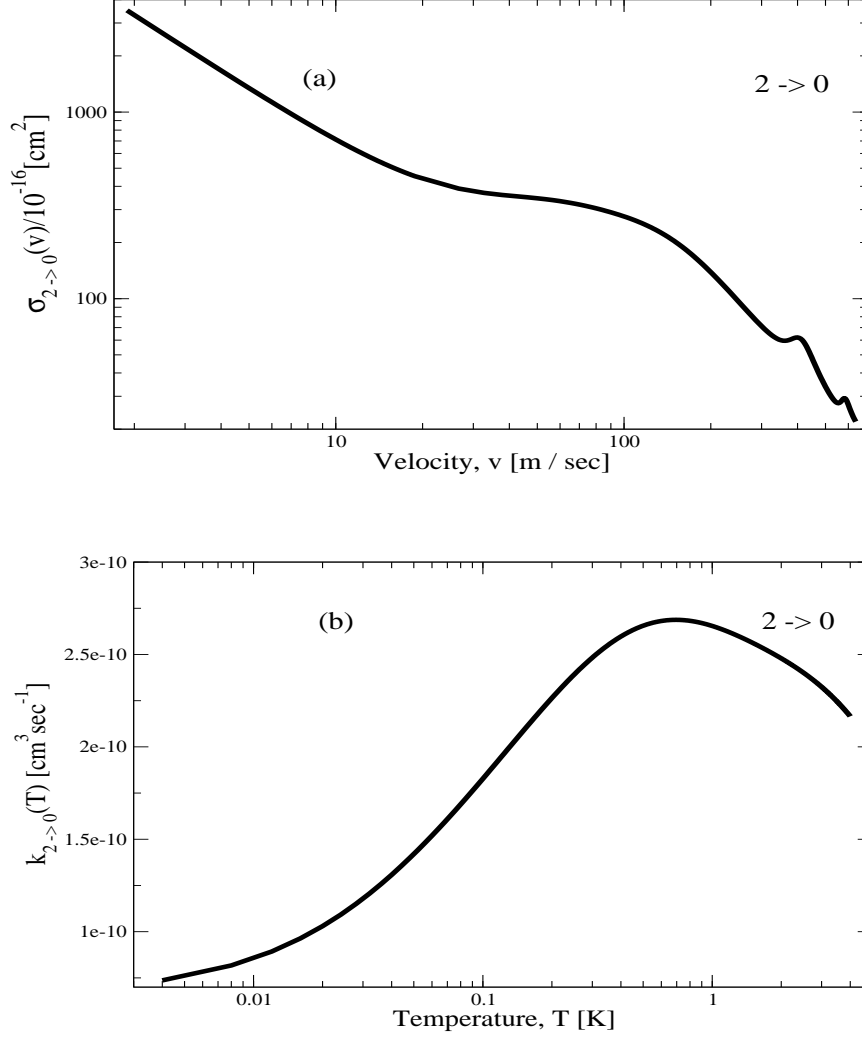


FIG. 5: Upper plot (a): total state-resolved cross section $\sigma_{2 \rightarrow 0}(v)$ vs. velocity v . Lower plot (b): corresponding thermal rate coefficients $k_{2 \rightarrow 0}(T)$ vs. temperature T for the hydrogen molecule rotational relaxation process $\text{H}_2(j=2 \rightarrow j=0)$ in $\bar{\text{H}}\text{-H}_2$ collision.

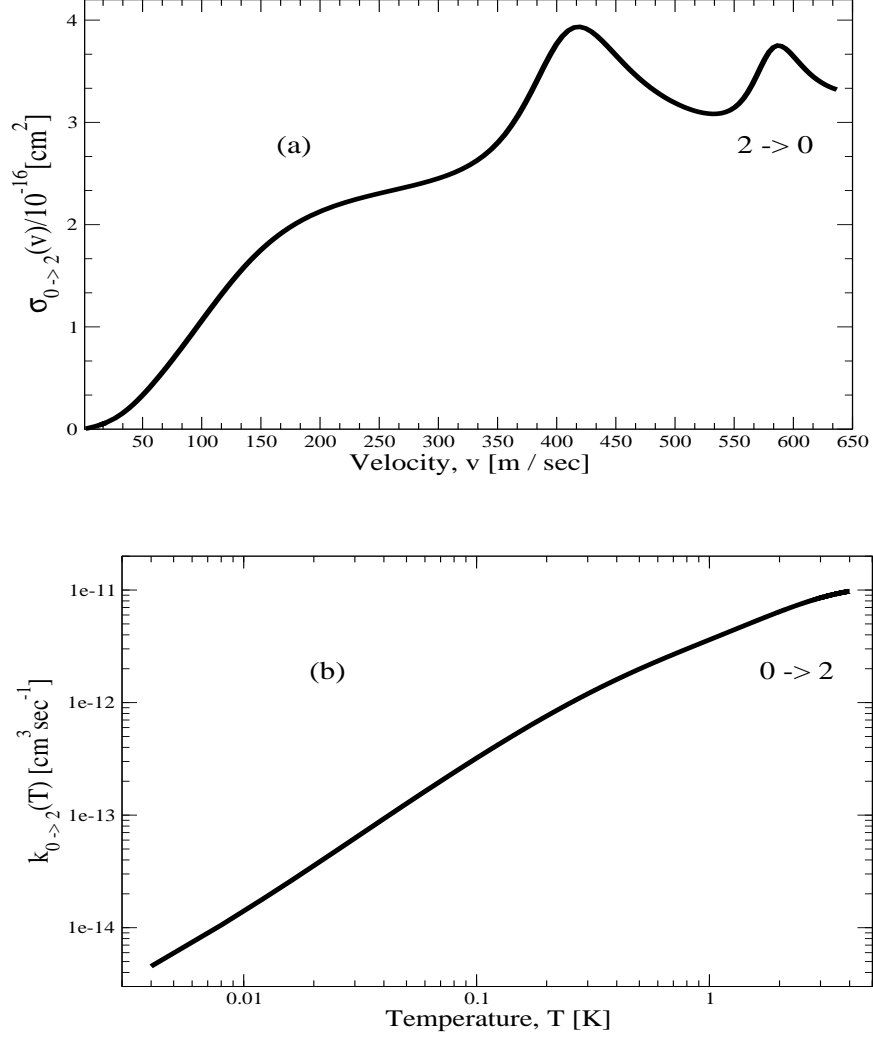


FIG. 6: Upper plot (a): total state-resolved cross section $\sigma_{0 \rightarrow 2}(v)$ vs. velocity v . Lower plot (b): corresponding thermal rate coefficients $k_{0 \rightarrow 2}(T)$ vs. temperature T for the hydrogen molecule rotational excitation process $\text{H}_2(j=0 \rightarrow j=2)$ in $\bar{\text{H}}\text{-H}_2$ collision.

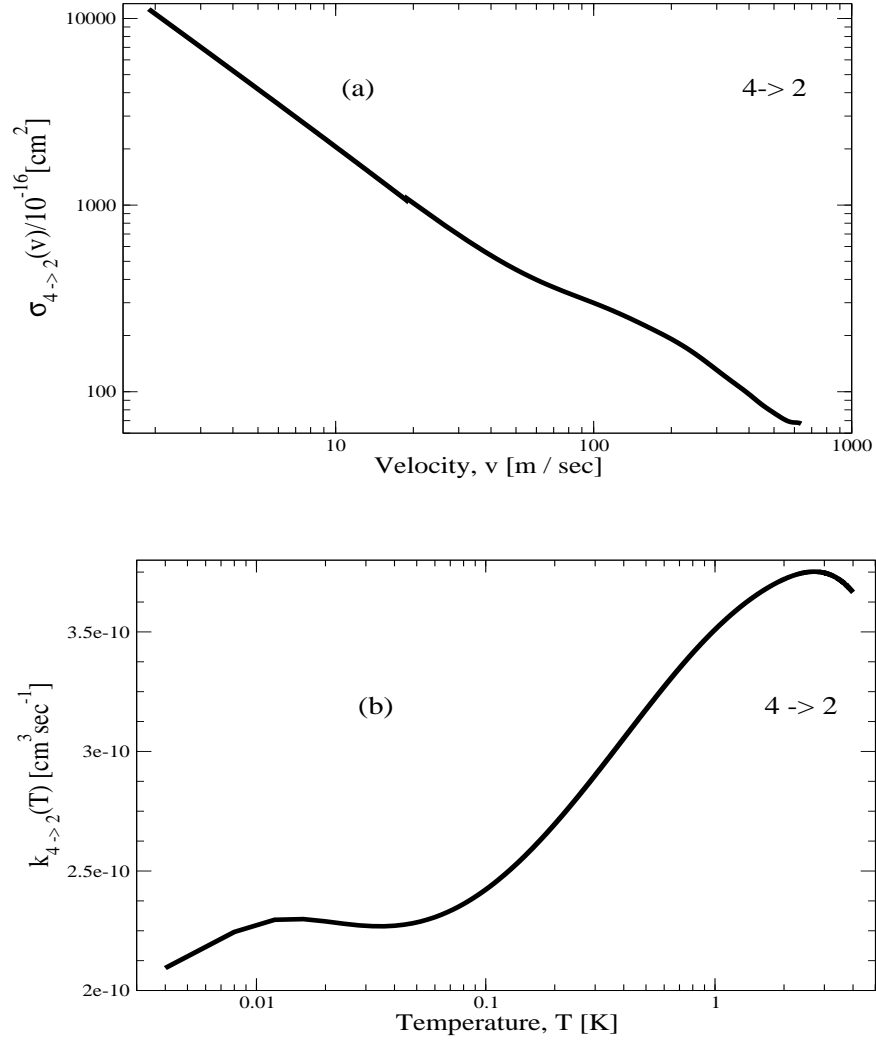


FIG. 7: Upper plot (a): total state-resolved cross section $\sigma_{4 \rightarrow 2}(v)$ vs. velocity v . Lower plot (b): corresponding thermal rate coefficients $k_{4 \rightarrow 2}(T)$ vs. temperature T for the hydrogen molecule rotational relaxation process $\text{H}_2(j=4 \rightarrow j=2)$ in $\bar{\text{H}}\text{-H}_2$ collision.

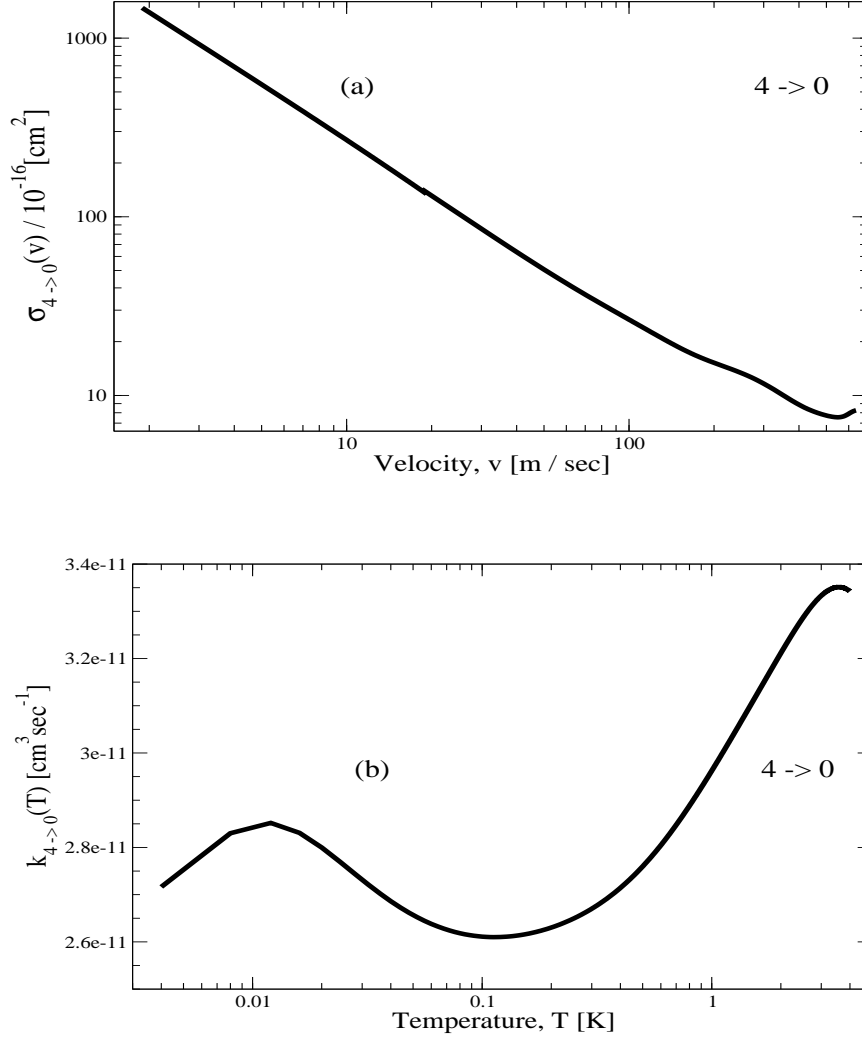


FIG. 8: Upper plot (a): total state-resolved cross section $\sigma_{4 \rightarrow 0}(v)$ vs. velocity v . Lower plot (b): corresponding thermal rate coefficients $k_{4 \rightarrow 0}(T)$ vs. temperature T for the hydrogen molecule rotational relaxation process $\text{H}_2(j=4 \rightarrow j=0)$ in $\bar{\text{H}}\text{-H}_2$ collision.